Molecular dynamics using quasielastic neutron scattering technique

S. Mitra and R. Mukhopadhyay*

Solid State Physics Division, Bhabha Atomic Research Centre, Trombay, Mumbai 400 085, India

Quasielastic neutron scattering (QENS) technique is well suited to study the molecular motions (rotations and translations) in solids or liquids. It offers a unique possibility of analysing spatial dimensions of atomic or molecular processes in their development over time. We describe here some of the systems studied using the QENS spectrometer, designed, developed and commissioned at Dhruva reactor in Trombay. We have studied a variety of systems to investigate the molecular motion, for example, simple molecular solids, molecules adsorbed in confined medium like porous systems or zeolites, monolayer-protected nanosized metal clusters, water in Portland cement as it cures with time, etc.

NEUTRON scattering is a powerful experimental tool for studying the structure and dynamics of atoms and molecules in condensed matter[1,2]. This is possible as neutron has a wavelength matching with the inter-atomic spacings in solids and also its energy is close to the excitations in the solid. It is particularly suited for studying the dynamics of protons because of the large scattering cross-section of the latter compared to that of other elements ($\sigma_H \sim 81$ barns, $\sigma_{\text{other elements}} \sim 4$–5 barns). Inelastic neutron scattering experiments are used either for studying the periodic motions like vibrations or for studying the thermally activated single-particle motions which show up in Doppler-broadened elastic lines. The latter are studied using a technique known as the quasi-elastic neutron scattering (QENS). It offers a unique possibility of analysing spatial dimensions of atomic or molecular processes in their development over time. The timescale of the dynamical motion, its geometry as well as the nature of the hindering potential can all be obtained from the neutron scattering experiments, which are carried out using either a triple axis or a time-of-flight spectrometer[1]. A few examples of molecular motion studies in various solids and liquids using QENS technique can be found elsewhere[3–5].

In a medium flux reactor like Dhruva, data acquisition time in a conventional spectrometer is rather long. It is always desired to reduce the data acquisition time for a good enough statistics in an inelastic neutron scattering experiment. We have adopted the design of a spectrometer developed at Risö, Denmark, known as MARX (Multi Angle Reflecting X-tal) spectrometer. Working principle of this spectrometer is similar to that of conventional triple axis spectrometer (TAS), but modified for a higher throughput[6]. The essential difference with the TAS is that the MARX spectrometer measures the scattered neutrons over a much larger solid angle than does a triple axis instrument.

The scattered neutrons are energy-selected by a large analyser crystal and detected using a position-sensitive detector. Thus an energy scale is set up along the detector and the MARX spectrometer provides a complete energy spectrum for one instrumental configuration. This spectrometer is installed at the end of the through tube (which is designed to provide high thermal neutron flux with minimum gamma and fast neutron components) at Dhruva reactor, Trombay. The higher thermal neutron intensity and use of MARX-mode make this a well-suited instrument for neutron quasielastic scattering experiments. A double monochromator used in tandem for variation of incident energy, placed inside the biological shield unlike a conventional instrument, provides a closer approach to the source and gives higher intensity at the sample position. By virtue of the double monochromator, neutrons with different incident energies can be obtained at the same sample position. The out-of-pile portion of the spectrometer is situated on a 'tanzboden' (dance floor). The spectrometer is manoeuvred on air cushion. Another feature of the spectrometer is that it is of modular type; there is a provision to alter the distance between the different axes and thus one can obtain different energy resolutions.

The main features of the double crystal monochromator are: (i) two crystals in parallel geometry set at Bragg angles for the required incident energy and in tandem, (ii) capability of these crystals to rotate about vertical axes and to translate with respect to each other, and (iii) the in-pile beam shield within the biological shield. The second crystal of the double monochromator assembly is vertically bent to focus the neutrons at the sample position. The out-of-pile portion of the spectrometer is on the air cushion. The sample table, analyser mount and detector are supported by air pads on machined and polished MS plates that act as the floor for the air cushion. The spectrometer is fabricated at the BARC workshops. A schematic diagram of the instrument is given in

*For correspondence. (e-mail: mukhop@apsara.barc.ernet.in)

Figure 1. Photograph of the spectrometer is shown in Figure 2. Details of this spectrometer can be found elsewhere[7].

Instrumental resolution is experimentally obtained from the measured full width at half maximum (FWHM) of the spectrum from a vanadium sample. It is found that for neutrons of incident energy of 5.1 meV, the instrument has energy resolution of 200 μeV, which agrees well with the theoretically calculated value. The corresponding time window of the spectrometer is 10–20 ps, or equivalently, diffusion constant of the order of 10^{-5} cm^2/s can be measured. The wave-vector transfer range covered by this spectrometer is 0.67–1.8 Å^{-1}.

Theoretical aspects

In a neutron scattering experiment the measured intensity is proportional to the double-differential cross-section[1],

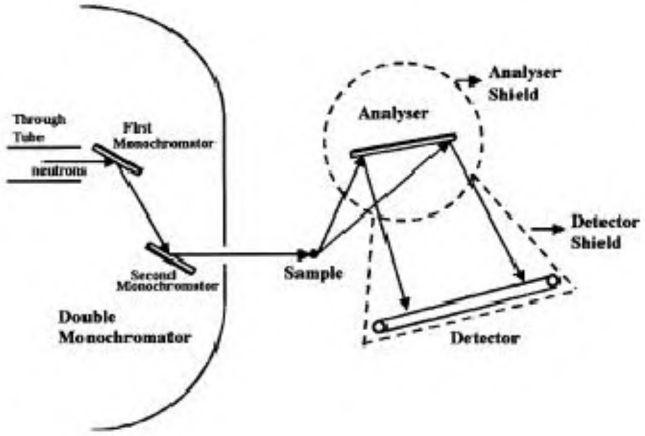

Figure 1. Schematic of QENS spectrometer at Dhruva.

Figure 2. Photograph of QENS spectrometer at Dhruva.

$$\frac{\partial^2\sigma}{\partial\omega\partial\Omega} \propto \frac{k}{k_0}[\sigma_{\text{coh}}\, S_{\text{coh}}(Q,\omega)+\sigma_{\text{inc}}\, S_{\text{inc}}(Q,\omega)], \qquad (1)$$

where σ is the scattering cross-section and $S(Q, \omega)$ is the scattering law. The subscripts coh and inc denote the coherent and incoherent components. $\boldsymbol{k}$ and $\boldsymbol{k}_0$ are the final and initial wave vectors respectively, and $\boldsymbol{Q}$ (= $|\boldsymbol{k}-\boldsymbol{k}_0|$) is the momentum transfer. ω is the angular frequency corresponding to energy transfer $\hbar\omega = E - E_0$, where E and E_0 are the scattered and incident energies respectively. Protons have a large incoherent neutron scattering cross-section (~ 80 barns compared to their coherent part of 1.7 barns, total cross-section of C, O and N being 5.5, 4.2 and 12.4 barns respectively). Therefore, in a neutron scattering experiment from a protonated system, the observed dynamics mainly corresponds to the incoherent part only. For a molecular system different kinds of motions – translational, rotational and vibrational – can exist, and generally it is assumed that these motions are dynamically independent (for mathematically tractable solution). In the quasielastic regime (within ± 2 meV of the elastic line) the vibrational contribution is related to the Debye–Waller factor, e^{-2W}, $W = \frac{1}{2}\langle u^2\rangle Q^2$, where $\langle u^2\rangle$ is the mean square displacement of the scattering atom. The total $S(Q, \omega)$ can be expressed as a convolution of the respective scattering functions,

$$S_{\text{inc}}(Q,\omega) = \exp\left(-\langle u^2\rangle Q^2\right)\left[S_{\text{inc}}^{\text{rot}}(Q,\omega)\otimes S_{\text{inc}}^{\text{trans}}(Q,\omega)\right]. \qquad (2)$$

The rotational incoherent scattering law can be written as[1],

$$S(Q,\omega) \propto A(Q)\delta(\omega)+[1-A(Q)]L(\sqrt{},\omega), \qquad (3)$$

where the first term is the elastic part and the second, the quasielastic one. $L(\Gamma, \omega)$ is a Lorentzian function,

$$L(\sqrt{},\omega) = \frac{1}{\pi}\frac{\sqrt{}}{\sqrt{}^2+\omega^2}, \qquad (4)$$

where Γ is the half width at half-maximum (HWHM) of the Lorentzian function inversely proportional to the reorientation time τ. It is convenient to analyse the data in terms of elastic incoherent structure factor (EISF), which provides information about the geometry of the molecular motions. If $I_{\text{el}}(Q)$ and $I_{\text{qe}}(Q)$ are the elastic and quasielastic intensities respectively, then EISF is defined as[1],

$$\text{EISF} = \frac{I_{\text{el}}(Q)}{I_{\text{el}}(Q)+I_{\text{qe}}(Q)}. \qquad (5)$$

Therefore, $A(Q)$ in eq. (3) is nothing but the EISF. The quasielastic part may arise due to rotational or translational motions of the particles.

As far as rotation is concerned, a molecule can rotate about any of its axes and different models can be envis-

aged to describe the motion. We discuss below some of these models:

Isotropic rotational diffusion

In this model, molecular reorientation is assumed to take place through small-angle random rotations. Then, on a time average, no orientation is most probable. It has been shown by Sears[8] that the incoherent scattering law for a scattering particle undergoing isotropic rotational diffusion on the surface of a sphere of radius a with rotational diffusion coefficient D_R, can be written as,

$$S(Q,\omega) = A_0(Q)\delta(\omega) + \sum_{l=1}^{l=\infty} A_l(Q)\frac{1}{\pi}\frac{l(l+1)D_R}{[l(l+1)D_R]^2+\omega^2}, \quad (6)$$

where

$$A_0(Q) = j_0^2(Qa) \text{ and } A_l(Q) = (2l+1)j_l^2(Qa), \quad (7)$$

where j_l is the lth spherical Bessel function.

Uniaxial rotational diffusion

If a cylindrical molecule undergoes rotational diffusion about the long axis of the molecule, the scattering law retains the form of a delta function plus a series of Lorentzian functions[1], but it depends on the angle θ between $\boldsymbol{Q}$ and the director $\boldsymbol{n}$ (defining the orientation of the molecule),

$$S(Q,\omega) = J_0^2(Qa\,\mathrm{Sin}\theta)\delta(\omega) + 2\sum_{l=1}^{l=\infty} J_l^2(Qa\,\mathrm{Sin}\theta)\frac{1}{\pi}\frac{D_R l^2}{(D_R l^2)^2+\omega^2}, \quad (8)$$

where a is the radius of the circle and the J_ls are Bessel functions of the first kind. The behaviour of the elastic and the quasielastic structure factors strongly depends on the angle θ between the direction of **Q** and the axis of rotation. For a powder sample, one has to take an isotropic average over angle θ. No formal expression exists for the average. However, it is possible to use expressions of the structure factors for a jump diffusion model over N equally spaced sites, where N is sufficiently large.

Jump model among N equivalent sites on a circle

In this model it is assumed that the motion is by jumps of angle α and characteristic time τ. It is also assumed that the jump time is much shorter compared to the residence time of the particle at a particular site τ. For a particle which is allowed to perform a random walk among N equivalent sites, jumps being restricted to neighbouring sites only, the expression for the scattering law for a powder sample[9] is

$$S(Q,\omega) = A_0(Q)\delta(\omega) + \sum_{l=1}^{N-1} A_l(Q)\frac{1}{\pi}\frac{\tau_l}{1+\omega^2\tau_l^2}, \quad (9)$$

with

$$A_0(Q) = \frac{1}{N}\sum_{n=1}^{N} j_0(Qa_n) \text{ and}$$
$$A_l(Q) = \frac{1}{N}\sum_{n=1}^{N} j_0(Qa_n)\cos\left(\frac{2\ln\pi}{N}\right). \quad (10)$$

The a_n are the jump distances under the effect of $(2n\pi/N)$ rotations and can be written as

$$a_n = 2a\sin\left(\frac{n\pi}{N}\right). \quad (11)$$

The residence times can be evaluated from

$$\tau_l^{-1} = 2\tau^{-1}\sin^2\left(\frac{\pi l}{N}\right). \quad (12)$$

If the number of sites over which jumps occur is sufficiently large, the scattering function for a jump mode is nearly identical to that of a uniaxial rotational diffusion[10] in the limit of $Qa < \pi$. Under these conditions, the rotational diffusion constant D_R can be identified with the jump rate probability $1/\tau_l$ obtained from eq. (12), i.e.

$$D_R = \frac{1}{\tau_1} = \frac{2}{\tau}\sin^2\left(\frac{\pi}{N}\right). \quad (13)$$

To describe translational motion, the different models used are:

Continuous free diffusion

The simplest motion that can be thought is the Brownian motion where it is assumed that the particles move under the influence of forces arising from the collisions between them. Between two collisions, particles move in straight lines. After a collision, the particle gets scattered into a random direction, independent of the previous one. In this case, incoherent scattering law can be calculated by solving Fick's law[1] and written as

$$S_{\mathrm{inc}}(Q,\omega) = \frac{1}{\pi}\frac{DQ^2}{\omega^2+(DQ^2)^2}. \quad (14)$$

The scattering law exhibits a Lorentzian shape whose HWHM increases with the momentum transfer according to a DQ^2 law, and provides a direct method of determining the diffusion constant.

Jump diffusion model

In case of Brownian motion, the jump length l of the diffusing particle is assumed to be small. In other words,

diffusion is assumed to occur via infinitely small, elementary jumps. This assumption is satisfied if we are concerned only with small $\boldsymbol{Q}$ values where the exact mechanisms of diffusion are not revealed and Fick's law is satisfied. At large momentum transfers, the continuous diffusion model appears no more true, and we need to describe the diffusion process in more detail.

Chudley–Elliott model: One such model was formulated by Chudley and Elliott[11] who assumed that for a time interval τ, an atom remains on a given site, vibrating about a centre of equilibrium, building up a thermal cloud. After this time, the atom moves rapidly to another site, in a negligible jump time. The jump length l is assumed to be the same for all such jumps under consideration. This model is also called a fixed jump model. The powder-averaged scattering law in this case can be written as

$$S_{\text{inc}}(Q,\omega) = \frac{1}{\pi}\frac{\sqrt{(Q)}}{\omega^2 + (\sqrt{(Q)})^2}, \tag{15}$$

where

$$\sqrt{(Q)} = \frac{1}{\tau}\left[1 - \frac{\sin Ql}{Ql}\right]. \tag{16}$$

The diffusion constant D is given by Einstein's relation

$$D = \frac{l^2}{6\tau}. \tag{17}$$

Hall–Ross model: In this model, Hall and Ross[12] assumed a jump diffusion model where the jump length is not fixed; instead it is Gaussian distributed. Scattering law in this case can be written as

$$S_{\text{inc}}(Q,\omega) = \frac{1}{\pi}\frac{\sqrt{(Q)}}{\omega^2 + (\sqrt{(Q)})^2}, \tag{18}$$

where

$$\sqrt{(Q)} = \frac{1}{\tau}\left[1 - \exp\left(-\frac{Q^2\langle l^2\rangle}{6}\right)\right]. \tag{19}$$

Here, τ is again the time which the particle spends at a particular site before jumping to another site and is called residence time. $\langle l^2\rangle^{0.5}$ is the root mean square jump length. The diffusion constant D can be evaluated using eq. (17).

In any scattering experiment, the measured data are the convolution product of the scattering function with the resolution function of the instrument. The resolution function in a (QENS) experiment is determined by measuring scattering from a standard sample like vanadium or ZrH_2. To analyse the QENS data it is customary to assume a model scattering function, convolute the scattering function with the instrumental resolution function and then obtain the dynamical parameters involved in the model scattering function by least squares fit to the experimental data.

Some typical systems studied using this spectrometer are discussed below.

Examples

Molecular motions of hydrocarbons adsorbed in zeolites

The investigation of molecular migration of sorbate and reactant molecules in zeolites is an important topic in both fundamental research and in industrial applications. The role played by the pore geometry and framework acid sites of zeolites in the catalytic activity and selectivity of these materials is under extensive investigation. Dynamics of the guest molecule depends on the shape and size of the host zeolitic system. With a view to understand the dynamics and binding states of various hydrocarbon molecules adsorbed in the different-size pores in different zeolites, we have studied benzene in HZSM-5 and CaZSM-5 zeolites under ambient conditions and propane molecules in Na–Y zeolite at different temperatures.

Benzene in ZSM-5 zeolite: We consider two cases: (a) when the pore size is comparable to the size of the guest molecule and (b) when the host contains supercages and the guest molecules are comparatively small in size.

For the first case, we used ZSM-5 zeolite as the host and benzene as the guest molecule. In ZSM-5 zeolite there are two types of channels consisting of ten-membered oxygen rings. The straight elliptical channels (5.7–5.2 Å) are interconnected by near-circular channels (5.4 Å) in a zig-zag fashion, and there are four channel intersections per unit cell. Schematic of ZSM-5 zeolite is shown in Figure 3 *a*. Experiments were carried out with benzene (size ~ 5 Å) coverage of three molecules per unit cell of HZSM-5 and cation-exchanged CaZSM-5 zeolite.

Translational diffusion coefficients for benzene in ZSM-5 have been reported as 10^{-9}–10^{-10} cm^2/s from gravimetric measurements[13]. Translational motion due to small diffusion coefficients is not expected to contribute to the quasielastic profiles. Typical QENS data are shown in Figure 4. The observed quasielastic profiles are only due to rotational motion of the benzene molecules.

Elastic and quasielastic parts at all Q values were separated from the total spectra using eq. (3) as the model scattering law and EISF was determined. Figure 5 shows the extracted EISF at all the Q values for benzene in HZSM-5 and CaZSM-5 zeolite. The theoretical EISFs for a molecule undergoing jump diffusion among N equivalent sites on a circle[9] (curve A: $N = 2$ and curve B: $N = 6$; eq. (10) and for isotropic rotational diffusion[8] (curve C; eq. (7) are also shown in Figure 5. It is evident that experimental EISF closely follows the theoretical EISF for $N = 6$ or the six-fold jump model. This indicates that the benzene molecules in HZSM-5 and in CaZSM-5 are

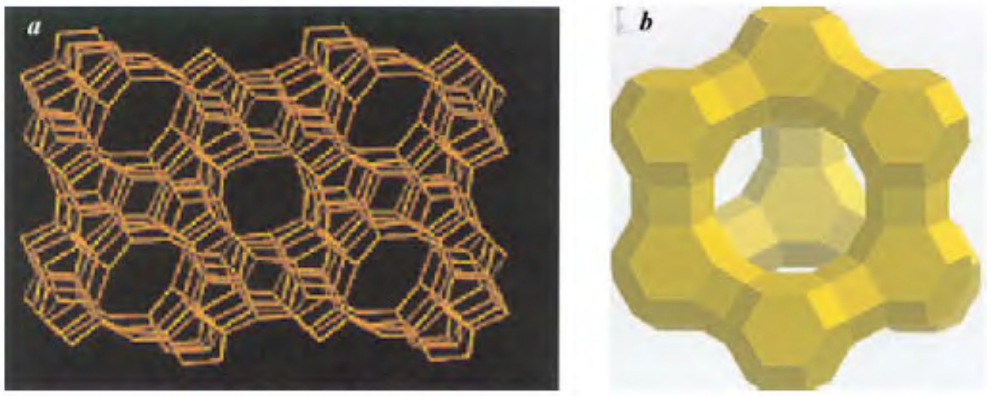

Figure 3. Schematic of cage structure in (*a*) ZSM-5 zeolite and (*b*) Na–Y zeolite.

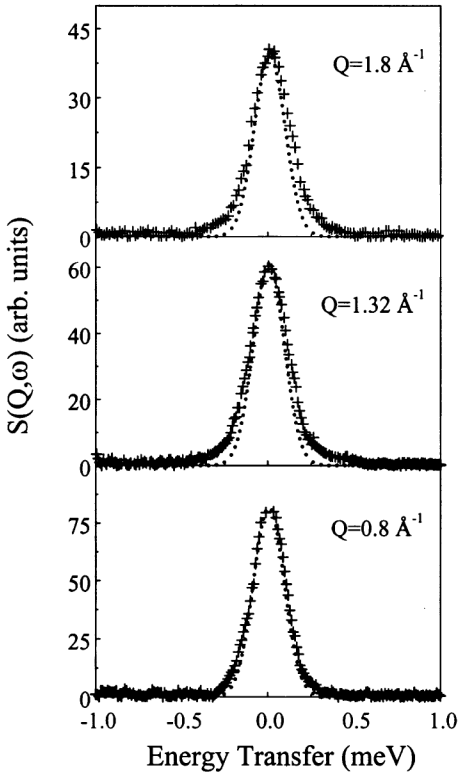

Figure 4. Typical QENS spectra at different Q values from benzene in HZSM-5. Instrumental resolution function is shown by dotted line.

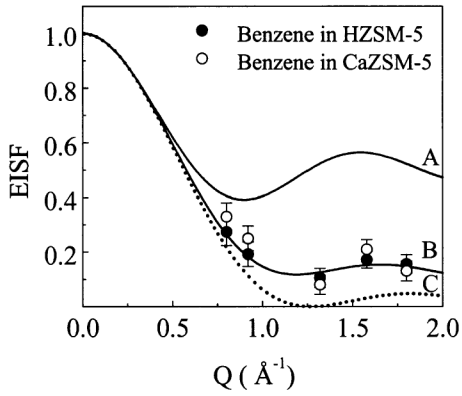

Figure 5. Variation of EISF with Q for benzene adsorbed in HZSM-5 and CaZSM-5 zeolite. Lines are the theoretical model calculations. A, Two-fold jump rotation model, B, six-fold jump rotation model; C, Isotropic rotational diffusion model.

performing six-fold jump rotations in the channel intersections.

To estimate the residence time τ of benzene molecule, the spectra were fitted with the scattering law for six-fold jump rotation (eq. (9)) convoluted with instrumental resolution. The fit was good at all the Q values. Figure 6 shows the quality of fit at some Q values. Quasielastic component is shown by a thick solid line and the instrumental resolution function is shown by a dotted line. The estimated residence times as obtained from eq. (12) are 16.5 and 30.0 ps for benzene adsorbed in HZSM-5 and CaZSM-5 zeolites respectively. It may be noted that residence time of bulk benzene in the liquid and solid phases is ~ 2.5 ps at room temperature[14] and ~ 19.2 ps (ref. 15) at 277 K respectively. Our value is close to that of the solid phase. Fourier Transform Infra-Red (FTIR) studies performed by us on the same sample confirmed that benzene in these zeolites experiences an effect of zeolitic wall pressure, thereby leading to strong intermolecular interaction and eventually giving rise to a solid-like state of benzene. Details are given in ref. 16.

Propane in Na–Y zeolite: For the second case, namely where the size of the molecule is smaller than the pore size, we used Na–Y as the host material and propane as the guest molecule. Na–Y zeolite structure is made up of a network of tetrahedrally connected pores (α-cages) of diameter ~ 11.8 Å. The pores are interconnected through windows of diameter ~ 8 Å. Schematic of Na–Y zeolite structure is shown in Figure 3 *b*. Samples with propane ('size'~ 6 Å) coverage of 4.5 molecules per zeolitic supercage were used for the experiment. It is found that the observed QENS broadening is compatible with the translational motion only, although it is an assumption to start with. Our recent molecular dynamics simulation

study showed that benzene molecules undergo fast rotational motion inside the cage of Na–Y zeolite. This fast motion is not expected to be observed in the present spectrometer. Analysis of the experimental data was attempted using several models of the dynamics, and it was found that a model of $S(Q, \omega)$ proposed by Hall and Ross[12] was adequate and consistent with experimental data. Figure 7 shows the extracted HWHM and the fit with eq. (19) at different temperatures. The values of residence time, root mean square jump length and diffusion constant are listed in Table 1. Detailed results on this can be found elsewhere[17].

Molecular motions in liquid crystal BBBA

Liquid crystals usually exhibit several mesophases differing by the degree of ordering of the molecules, and the dynamics of these molecules is influenced by transition from one phase to another. In this example we have shown how different parts of the liquid crystal butyloxybenzylidine butylanilene (BBBA) have contributed to the quasielastic spectra, and how the contributions are separated from each other. The molecular conformation of the compound is shown in Figure 8.

The mesomorphic behaviour displayed by these materials is as follows[18]:

$$K \xrightarrow{7C} S_B \xrightarrow{41C} S_A \xrightarrow{45C} N \xrightarrow{76C} I$$

(K: crystalline, S_B: Smectic B, S_A: Smectic A, N: Nematic, I: Isotropic phases).

The QENS experiments were performed on unoriented samples using the quasielastic spectrometer discussed above. The quasielastic spectra were recorded in the wavevector transfer range (Q) of 0.8 to 1.8 Å^{-1}, in both smectic A and smectic B phases, i.e. at temperatures 300 and 316 K. The quasielastic part may arise due to translational or rotational motion of the particles. The translation motion is not expected to contribute in the present experiment, as the time window associated with the instrumental resolution is beyond the timescale involved. In fact, NMR relaxation-time studies have shown that the translational diffusion constant varies in the range of 1×10^{-11} to 1×10^{-18} m^2/s, which is well outside the time window of QENS. As far as rotation is concerned, some of the important reorientational dynamics in liquid crystals are: (i) reorientations around short axis of the molecule, (ii) reorientations along the long axis of the molecules and (iii) reorientations of the end chains. However, the rotations about the short axes are relatively slow due to highly anisotropic shape of the molecule and, in fact, fall into the NMR time window in the nematic phase itself. This dynamics, thus, should be even slower in the smectic phases. Therefore, the dynamics that may fall into QENS time window includes rotations of the molecules about their long axis and reorientations of the end chains.

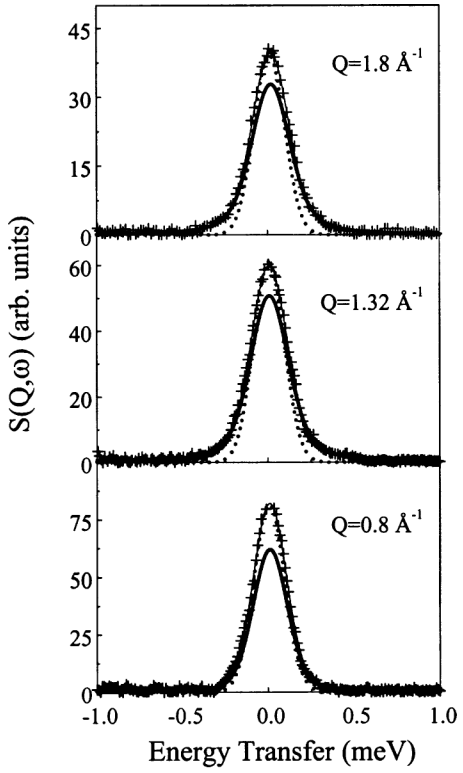

Figure 6. Typical fit of QENS spectra from benzene in HZSM-5 using eq. (9) with $N = 6$ at different Q values. (—), Total fit; (—), Quasielastic component; and (.....) Instrumental resolution.

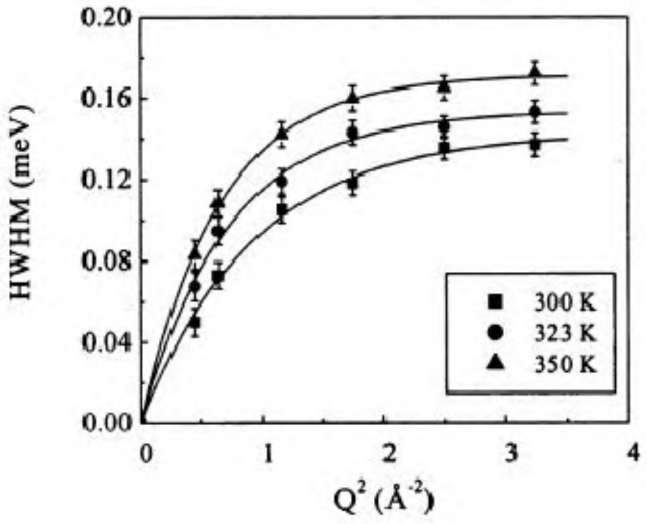

Figure 7. Variation of HWHM of quasielastic component with Q for propane in Na–Y zeolite. Solid lines are the fit with Hall and Ross model (see text).

Table 1. Values of residence time, mean jump length and diffusion constant of propane in Na–Y zeolite at different temperatures

T(K)	τ (ps)	$\langle l^2 \rangle^{0.5}$ (Å)	D (× 10^{-5} cm^2/s)
300	4.6 ± 0.5	2.5 ± 0.2	2.3 ± 0.3
323	4.3 ± 0.4	2.9 ± 0.2	3.2 ± 0.3
350	3.8 ± 0.3	3.0 ± 0.3	4.0 ± 0.4

Different types of rotations in the molecule can be envisaged: (a) Coregroup rotates about the long axis of the molecule with the end chains remaining static. (b) Only the end chain cylinders rotate, but the core group remains static. (c) Both the core group and the end chain rotate independent of each other.

In Figure 9 the experimentally obtained EISF values at 300 K, 316 K and the theoretically calculated EISF from different models are plotted. As a molecule rotates about an axis, the associated atoms will rotate, on an average, on the surface of a circle. Curve (a) represents the calculated EISF (eq. (10)) for model A considering jump diffusion among N equivalent points on a circle of radius 2.5 Å (ref. 9) with $N = 12$. Curve (b) is the EISF for model B considering jump diffusion ($N = 12$) model taking the radius as 1.4 Å. Curve (c) represents the calculated EISF for model C taking the radius as 1.4 Å in the case of end-chain rotation and 2.5 Å in the case of core-group rotation, considering the jump diffusion ($N = 12$) model. The value of a as 1.4 Å for end-chain rotation is chosen because it is seen that only this value of a can give a consistent result while fitting the spectra with full scattering law for all the Q values. It is clear from Figure 9 that the curve (c) closely follows the experimental EISF well at both the temperatures. This indicates the validity of the model (C), i.e. there are two types of cylinders rotating with different timescales, one with a radius of rotation 2.5 Å and the other with 1.4 Å, at both the phases.

The reorientation times, τ_1, at 300 K in the smectic B phase is obtained to be 6.1 ($\pm$ 1.6) $\times$ 10^{-11} s and 1.8 ($\pm$ 0.6) $\times$ 10^{-11} s, for the core-group and end-chain respectively. In the smectic A phase (316 K), the corresponding reorientation times are 4.1 ($\pm$ 1.2) $\times$ 10^{-11} s and 1.6 ($\pm$ 0.5) $\times$ 10^{-11} s. Detailed report on this work can be found elsewhere[19].

Akyl chain dynamics in monolayer protected clusters

Study of the structure and properties of ultra-thin films at interfaces has advanced at a rapid pace, with their potential applications in the fields of optoelectronics and molecular engineering[20]. These ordered films have been classified into Langmuir–Blodgett films and self-assembled monolayers (SAMs) – the molecular assemblies which form spontaneously by immersion of an appropriate substrate into a solution of active surfactant. Classification of the structure and properties of SAMs is based on dimensionality, i.e. 2D SAMs and 3D SAMs. The 2D SAMs are ordered molecular assemblies formed by the adsorption of an active surfactant on a planar solid substrate. The 3D SAMs are monolayers of surfactants formed on a nano-sized metal core; the whole system together is called the monolayer protected metal clusters (MPCs). Figure 10 *a* shows the schematic of an isolated MPC system. The alkyl chains are seen diverging as they move away from the core. Interdigitation among individual monolayers of the neighbouring clusters results in a superlattice structure (Figure 10 *b*).

In the present study, our objective was to understand the dynamics of alkyl chains in the MPCs, especially when they go through a phase transition. The systems chosen are octadecanethiol-capped gold cluster (AuC_{18}) and octanethiol-capped silver cluster (AgC_8). While the monolayer assembly around the cluster in the former is near perfect with all-*trans* conformation, the latter exhibits a superlattice assembly. Results from a 2D-SAM (a layered thiolate: AgC_{12}) are also presented for comparison.

In MPCs, the hydrogen atoms are attached to the alkyl chains and the chains are fixed on the metal core. Therefore, no translational motion of hydrogen atoms is expected. The observed dynamics should be related to the rotational motion of the alkyl chains only.

Rotation of the alkyl chains may be described by either jump diffusion[9] or uniaxial rotational model[1]. However, the structure factor for jump diffusion with N equivalent sites ≥ 6 becomes indistinguishable from the uniaxial model. The data were first separated into elastic and quasi-elastic components and from the extracted EISF, the plausible model was chosen.

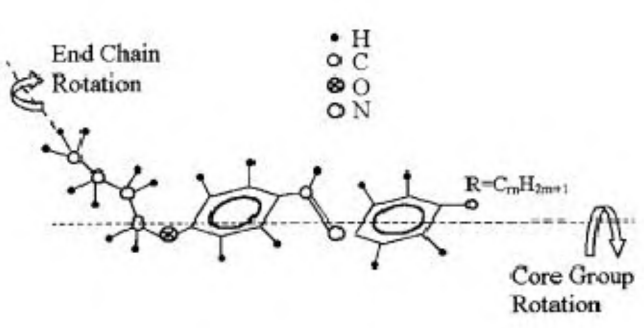

Figure 8. Molecular conformation of BBBA compound.

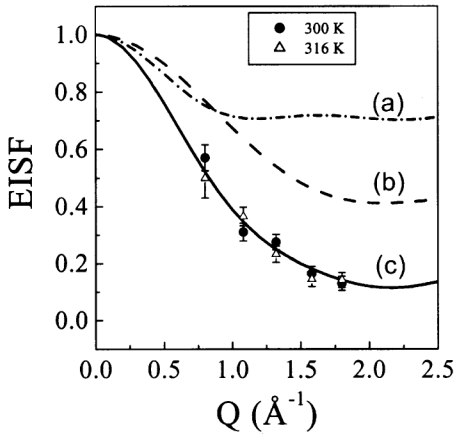

Figure 9. Variation of EISF with Q for liquid crystal BBBA at temperatures 300 and 316 K. Lines are the theoretically calculated EISFs; (a) Model A; (b) Model B; (c) Model C (see text).

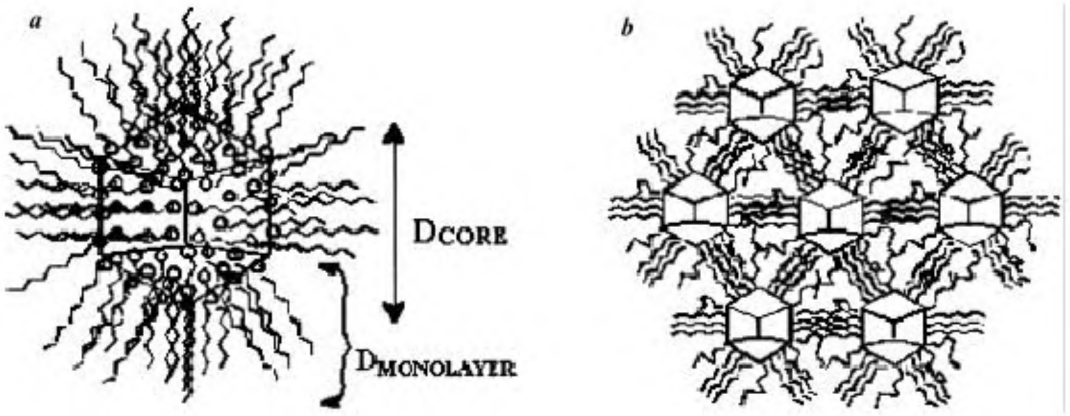

Figure 10. ***a***. Schematic of a monolayer protected cluster (MPC). Diameter of the core (D_{CORE}) is in the range of 30 Å and thickness of the monolayer ($D_{MONOLAYER}$) here is ~ 9 Å. Alkyl chains are seen diverging as they move away from the core. ***b***, Schematic of the superlattice assembly of MPCs. Interdigitation between neighbouring clusters is seen.

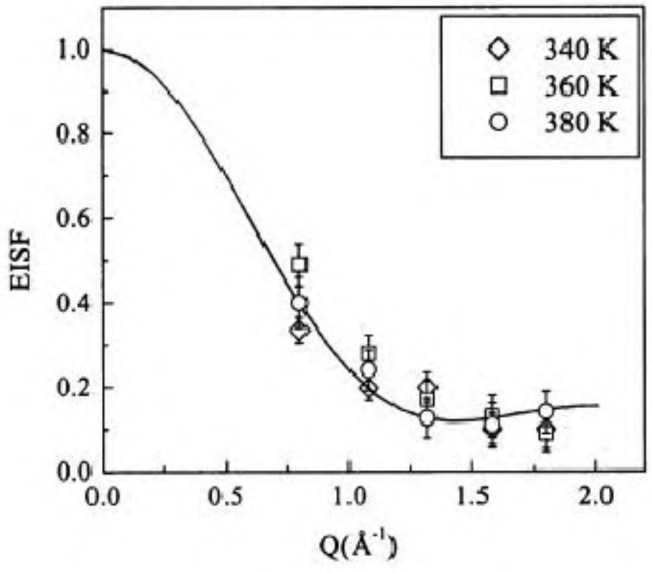

Figure 11. Variation of EISF with Q for AuC_{18} at different temperatures. Solid line corresponds to the calculation for uniaxial rotational diffusion model.

Octadecanethiol-capped gold cluster (Au-$SC_{18}H_{37}$): It is found that gold clusters do not form superlattice structure[21]. Differential Scanning Calorimetry (DSC) showed phase transition related to the alkyl chain melting[21] at T_c (~ 333 K). QENS data show no quasielastic (QE) broadening below T_c in concurrance with the DSC results. However, broadening was observed at $T > T_c$. Extracted EISF for different temperatures is shown in Figure 11. Data have been consistently described on the basis of the jump model with $N = 6$ (eq. (10)) or uniaxial rotation model (solid line in Figure 11). It may be noted that the EISF is a function of the radius of gyration, and a value of 2.1 Å explains the data quite well. An activation energy of rotation equal to 6.3 ± 0.4 kcal/mol has been obtained from the temperature dependence of the residence time using Arrhenius law.

Octanethiol-capped silver cluster (Ag-SC_8H_{17}): QE broadening was observed below T_c also; however, it was found that all the molecules are not contributing to the dynamics up to a temperature of 360 K. The experimentally extracted EISF at different temperatures are shown in Figure 12. Assuming a fraction of number of protons, p_x, participating in the dynamics, the effective elastic fraction can be written as;

$$\mathrm{EISF}_{\mathrm{eff}} = [p_x A(Q) + (1 - p_x)], \tag{20}$$

where $A(Q)$ is the EISF according to the model. p_x is determined by least squares fit to the experimental data, assuming jump diffusion with $N = 6$ or uniaxial rotation model. The lines in Figure 12 correspond to the fitted ones. AgC_8 forms a superlattice structure and this is by virtue of chain interdigitation among the neighbouring clusters (Figure 10 *b*). The fact that $p_x = 0.5$ or 50% of the protons are participating in the dynamics in the temperature range 300–360 K, is in accordance with the structural conformation. For a simple cubic lattice and nearly spherical cluster geometry (actually truncated icosahedron), only those chains along the unit cell axes are interdigitating. This would permit only about half the chains to be free and others to interact quite strongly. However at 380 K, the value obtained for p_x is 1, suggesting that almost all the chains are contributing to the dynamics. This being closer to the melting point, the chains, which were earlier held fixed due to interdigitation, now have enough energy to be dynamic.

Layered thiolate (AgC_{12}): QE broadening was observed only above the melting temperature, T_m (400 K). Experimental EISF is consistent with the six-fold jump model. The dynamical parameters as obtained from the QENS measurements at different temperatures for the different samples are given in Table 2. Detailed report on the work can be found elsewhere[22].

State of water molecules in hydrated Portland cement

Portland cement is of immense use as a construction material. When mixed with water the slurry can be easily handled, which then hardens into a load-bearing structure. The major objective of the cement industry is to control this setting process to achieve the highest strength in the shortest period of time. For this, accurate knowledge of the hydration kinetics is required.

Anhydrous Portland cement mainly consists of tri-calcium silicate (C_3S), di-calcium silicate (C_2S) and tri-calcium aluminate (C_3A). When mixed with water, C_3S and C_2S react to form calcium silicate hydrate (C–S–H) and calcium hydroxide (CH). Although the water content in C–S–H is not known, it is believed that part of it is in the form of OH^- groups in the structure of the gel and the remainder is in the form of immobilized water molecules. C–S–H appears first as colloidal particles that proceed to link together and eventually form a gel-like structure. The microstructure determines the properties of the hardened concrete. Although this general process has been known for a long time, the state of water molecules within the hydrated structure remains uncertain. As mentioned earlier, QENS technique is effective to probe proton dynamics; therefore it can be suitably used to study the state of the water molecules after mixing with the cement. We have carried out QENS experiments on Portland cement to obtain information on the state of water molecules as time progresses after mixing it with Portland cement. Data were recorded from the zero hour (when the mixture was made) and continued up to 250 days. In the initial period (1st day), data were collected every 3 h and thereafter at suitably longer intervals. Typical QENS data at different times are shown in Figure 13. As can be seen from Figure 13, the intensity towards elastic scattering increases with time. Elastic intensity

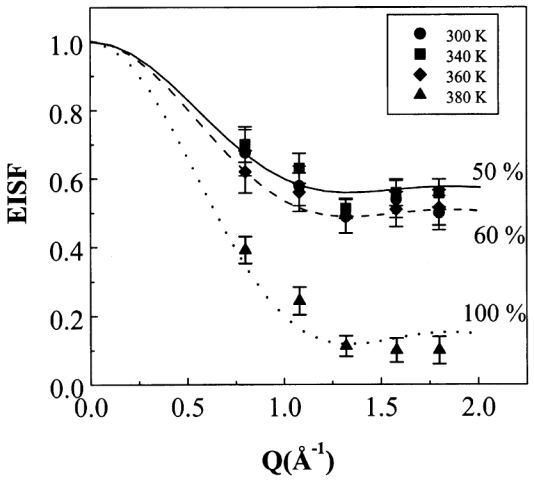

Figure 12. Variation of EISF with Q for AgC_8 at different temperatures. Lines correspond to the calculation for uniaxial rotational diffusion model with different proportions of alkyl chain contributing to the dynamics.

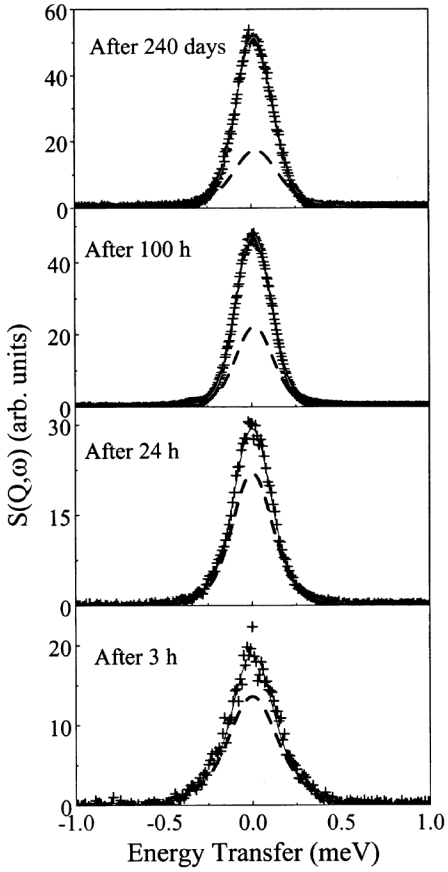

Figure 13. Typical QENS spectra at $Q = 1.32$ Å^{-1} at different times after hydration of Portland cement. Solid line is the fit to the data (+) using eq. (21), while dashed line is the quasielastic component.

Table 2. Parameters as obtained from the QENS data, for the different systems studied at different temperatures

	AgC_8			AuC_{18}			AgC_{12}		
T(K)	τ (ps)	p_x	a(Å)	τ (ps)	p_x	a(Å)	τ (ps)	p_x	a(Å)
300	5.2 ± 0.7	0.50 ± 0.02	2.0 ± 0.1	–	–	–	–	–	–
340	3.7 ± 0.4	0.56 ± 0.02	2.0 ± 0.1	6.2 ± 0.7	1	2.1 ± 0.1	–	–	–
360	2.9 ± 0.3	0.57 ± 0.01	2.1 ± 0.1	3.7 ± 0.4	1	2.1 ± 0.1	–	–	–
380	4.1 ± 0.5	1.00 ± 0.02	2.0 ± 0.1	2.3 ± 0.3	1	2.1 ± 0.1	–	–	–
400	–	–	–	–	–	–	3.8 ± 0.4	1	2.2 ± 0.2

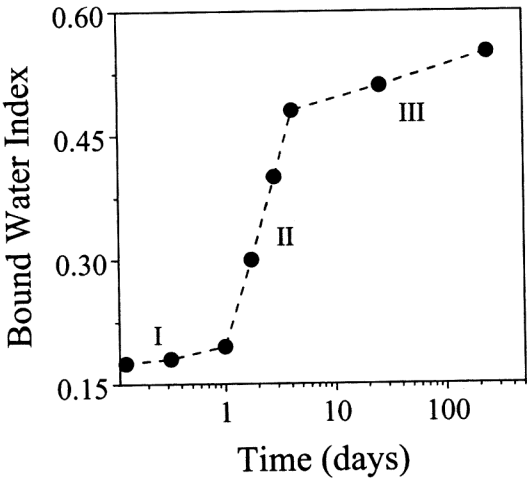

Figure 14. Variation of bound water index with curing time (as discussed in text). Dashed line is guide to the eye.

comes from the bound hydrogen. This means that as time progresses, more and more water molecules become bound and contribute towards the elastic line. In terms of a simplistic approach we have analysed the data to understand how the cement curates with time. The scattering function $S(Q,\omega)$ to describe the water dynamics can be written as:

$$S_{\text{inc}}(Q, \omega) = A(Q)\,\delta(\omega) + B(Q)\,L(\Gamma, \omega), \qquad (21)$$

where the first term accounts for the contribution from the bound hydrogen and the second term is that of the mobile hydrogen. The values of $A(Q)$ and $B(Q)$ are directly proportional to the amount of the bound and free hydrogen in the specimen respectively. The bound water index can be defined as:

$$I = \frac{A(Q)}{A(Q)+B(Q)}. \qquad (22)$$

Analysis of the data involves convolution of the scattering function (eq. (21)) with the instrumental resolution function and to obtain the parameters A, B and Γ by least squares fit with the experimental data. The typical fits are shown in Figure 13. The solid line is a fit to the data, while the dashed line is the Lorentzian component convoluted with the resolution function. It is clear from Figure 13 that as the time progresses, more water get immobilized and the intensity shifts from the Lorentzian to the Gaussian component, which means the proportion of elastic line increases. This is clearly reflected in Figure 14, where bound water index, as defined by eq. (22), is plotted with time.

As can be seen from Figure 14, variation of bound water index with time has three regimes – I: immediately after hydration (first day), when immobilization of the water molecules is rather slow, II: fast immobilization up to four days and III: in the bound state, when the process is slow again.

To conclude, the QENS spectrometer at Dhruva reactor has been used to study molecular dynamics in different systems, e.g. dynamics of different hydrocarbons in cages like zeolite, molecular reorientations of alkyl chains in MPCs, molecular reorientations in various organic and inorganic salts in different solid state environments, microemulsions, etc.

1. Bée, M., *Quasielastic Neutron Scattering*, Adam-Hilger, Bristol, 1988.
2. Press, W., *Single Particle Rotations in Molecular Crystals*, Springer, Berlin, 1981.
3. Mukhopadhyay, R., Mitra, S., Tsukushi, I. and Ikeda, S., *Chem. Phys. Lett.*, 2001, **341**, 45–50.
4. Mitra, S., Mukhopadhyay, R., Tsukushi, I. and Ikeda, S., *J. Phys.: Condens. Matter*, 2001, **13**, 8455–8465.
5. Mitra, S., Mukhopadhyay, R. and Chandrasekaran, K. S., *Physica B*, 2000, **292**, 29–34.
6. Kjems, J. K. and Reynolds, P. A., *Inelastic Neutron Scattering*, IAEA, Vienna, 1972, p. 733.
7. Mukhopadhyay, R., Mitra, S., Paranjpe, S. K. and Dasannacharya, B. A., *Nucl. Instrum. Methods A*, 2001, **474**, 55–66.
8. Sears, V. F., *Can J. Phys.*, 1966, **44**, 1999–2010.
9. Barnes, J. D., *J. Chem. Phys.*, 1973, **58**, 5193–5201.
10. Dianoux, A. J., Volino, F. and Hervet, H., *Mol. Phys.*, 1975, **30**, 1181–1188.
11. Chudley, G. T. and Elliott, R. J., *Proc. Phys. Soc.*, 1961, **77**, 353–365.
12. Hall, P. L. and Ross, D. K., *Mol. Phys.*, 1981, **42**, 673–682.
13. Zikanova, A., Bülow, M. and Schlodder, H., *Zeolites*, 1987, **7**, 115–127.
14. Winfield, D. J. and Ross, D. K., *Mol. Phys.*, 1972, **24**, 753–772.
15. Fujara, F., Petry, W., Schnauss, W. and Sillescu, H., *J. Chem. Phys.*, 1988, **89**, 1801–1806.
16. Tripathi, A. K., Sahasrabudhe, A., Mitra, S., Mukhopadhyay, R., Gupta, N. M. and Kartha, V. B., *Phys. Chem. Chem. Phys.*, 2001, **3**, 4449–4455; Mitra, S., Mukhopadhyay, R., Tripathy, A. K. and Gupta, N. M., *Appl. Phys. A*, 2002, 74[S], S1308–1310.
17. Mitra, S., Sayeed, A., Mukhopadhyay, R., Yashonath, S. and Chaplot, S. L., *Appl. Phys. A*, 2002, 74[S], S1317–1319; Sayeed, A., Mitra, S., Anil Kumar, A.V., Mukhopadhyay, R., Yashonath, S. and Chaplot, S. L., *J. Phys. Chem. B*, 2003, **107**, 527–531; Mukhopadhyay, R., Sayeed, A., Mitra, S., Anil Kumar, A. V., Yashonath, S. and Chaplot, S. L., *Phys. Rev. E*, 2002, **66**, 061121.1–061201.7.
18. Flannery, J. B. and Hans, W., *J. Phys. Chem.*, 1970, **74**, 3611; Smith, G. W. and Gardlund, Z. G., *J. Chem. Phys.* 1973, **59**, 3214–3228.
19. Mitra, S., Mukhopadhyay, R. and Venu, K., *Chem. Phys.*, 2000, **261**, 149–156.
20. Ulman, A., *An Introduction to Ultrathin Organic Films from Langmuir–Blodgett to Self Assembly*, Academic Press, New York, 1991.
21. Sandhyarani, N., Pradeep, T., Chakrabarti, J., Yousuf, M. and Sahu, H. K., *Phys. Rev.*, 2000, **62**, R739–R742; Sandhyarani, N., Pradeep, T., Antony, M. P. and Paneer Selvam, G. J. and Pradeep, T., *J. Chem. Phys.*, 2000, **113**, 9794–9803.
22. Mitra, S., Nair, B., Mukhopadhyay, R. and Pradeep, T., *J. Phys. Chem. B*, 2002, **106**, 3960–3967.

ACKNOWLEDGEMENTS. We acknowledge the cooperation received from Central Workshops, BARC during the design and fabrication of the instrument. We thank all our collaborators for their contributions in various studies reported here. The reviewing editor of *Current Science* has contributed significantly in improving the presentation of the paper.

Received 7 August 2002; revised accepted 16 November 2002